0031-3998/04/5603-0440
PEDIATRIC RESEARCH

Vol. 56, No. 3, 2004
Printed in U.S.A.

A Chicken Model for *DGCR6* as a Modifier Gene in the DiGeorge Critical Region

BEEREND P. HIERCK, DANIËL G.M. MOLIN, MARIT J. BOOT, ROBERT E. POELMANN, AND ADRIANA C. GITTENBERGER-DE GROOT

Department of Anatomy and Embryology, Leiden University Medical Center, 2300 RC Leiden, The Netherlands

ABSTRACT

DGCR6 is the most centromeric gene in the human DiGeorge critical region and is the only gene in the region with a second functional copy on a repeat localized more distally on chromosome 22. We isolated the chicken ortholog of *DGCR6* and showed an embryonic expression pattern that is initially broad but becomes gradually restricted to neural crest cell derivatives of the cardiovasculature. Retrovirus based gene transduction was used to deliver sense and antisense messages to premigrating neural crest cells *in vivo*. Embryos in which *DGCR6* expression was attenuated revealed cardiovascular anomalies reminiscent of those found in DiGeorge syndrome. Moreover, the expression profiles of three other genes from the DiGeorge critical region, *TBX-1*, *UFD1L*, and *HIRA*, were shown to be altered in this model. *TBX-1* and *UFD1L* levels were increased, whereas *HIRA* was decreased in the hearts and pharyngeal arches of embryos treated with antisense or partial sense constructs, but not with sense constructs for *DGCR6*. The expression changes were transient and followed the normal *DGCR6* expression profile. These data show that neural crest cells might have a role in the distribution of modulator signals to the heart and pharyngeal arches. Moreover, it shows a repressor function for *DGCR6* on the expression of *TBX-1* and *UFD1L*. For the first time, DiGeorge syndrome is shown to be a contiguous gene syndrome in which not only several genes from the critical region, but also different cell types within the embryo, interact in the development of the phenotype. **(*Pediatr Res* 56: 440–448, 2004)**

Abbreviations

DGS, DiGeorge syndrome
DORV, double outlet right ventricle
EGFP, enhanced green fluorescent protein
IAA-B, interruption of the aortic arch-type B
IRES, internal ribosomal entry site
ISH, *in situ* hybridization
LTR, long terminal region
NCC, neural crest cells
PFA, paraformaldehyde
PTA, persistent truncus arteriosus
VSD, ventricular septal defect

Congenital anomalies can provide important clues for the impact of specific processes in embryonic development. With respect to the chromosome 22 deletion syndrome or DGS (OMIM 188400), a patient's phenotype is clearly related to disturbance of migration or differentiation of neural crest. This might also be evoked by an inadequate interaction with surrounding cells like the endo- and mesoderm in the pharyngeal arches. In DGS patients, cardiovascular anomalies often coincide with thymic, thyroid, and parathyroid defects (1). All these areas are populated by cephalic and cardiac NCC that delaminate from the dorsal neural tube during neurulation and enter the mesodermal compartment of the embryo (2–5). The chicken NCC ablation model (6) shows that these neural crest areas are preferentially disturbed in DGS. In this respect, it is remarkable that, of the cardiovasculature in DGS patients, primarily the cardiac outflow tract and the fourth pharyngeal arch arteries are affected, although all arch arteries as well as outflow and inflow tracts of the heart are invaded by NCC (5, 7). The DGS phenotype in general presents with IAA-B, PTA, VSD, and tetralogy of Fallot (8, 9).

Although the affected chromosomal region has been known for over a decade, pinpointing the gene(s) involved in DGS is difficult. Genomic analysis of patients revealed a hemizygously typical deleted region of 1.5- to 3.0-Mb on chromosome 22q1.1 carrying over 30 genes. This region appears highly unstable due to the presence of AT-rich sequences (10) and low copy repeats (11). To date, four genes within this region have been described as candidate genes: *HIRA* (12), *UFD1L* (13, 14), *CRKL* (15), and *TBX-1* (16–18). Of these genes, *TBX-1* is the most promising, as hemizygously deleted mice show severe abnormalities in pharyngeal arch development (16). However, *Tbx-1* is not expressed in NCC, and, despite large-scale genetic

Received May 30, 2003; accepted April 5, 2004.
Correspondence: Adriana C. Gittenberger-de Groot, Ph.D., M.D., Department of Anatomy and Embryology, Leiden University Medical Center, P.O. Box 9602, 2300 RC Leiden, The Netherlands; e-mail: A.C.Gittenberger-de_Groot@LUMC.nl
Supported by a grant from the Netherlands Heart Foundation (NHS 98.082).

DOI: 10.1203/01.PDR.0000136151.50127.1C

screenings (18), only one patient has been described with a ~750-kb deletion that encompasses the 3' end of *TBX-1* (19). Possible explanations for these discrepancies are i) the involvement of embryonic cell types other than NCC in the etiology of DGS, ii) the presence of *cis*-acting elements in the *TBX-1* region regulating its expression "at distance" (20), or iii) modifier genes of the phenotype like *Vegf* (21) or *Fgf-8* (22–24). In fact, identification of haplo-insufficiency of genes on chromosome 22q11 in "nondeleted" DGS patients turns out to be extremely complicated. Besides the case mentioned above, this has only been described for one patient that was deleted in *UFD1L* and *CDC45L* (13).

Animal models have been described with DGS-type congenital cardiovascular malformations, but none of the genes involved localize to human chromosome 22q1.1. These models include null mutants for endothelin-1 (25), endothelin receptor-A (26), endothelin converting enzyme-1 (27), transforming growth factor β2 (28), mesenchyme forkhead genes *Mfh-1/Foxc2* (29) and *Mf-1/Foxc1* (30), *Pax3* (31), Semaphorin-3C (32), vascular endothelial growth factor (*VEGF165* (21)), and *Fgf-8* (22–24). Most likely, they represent downstream genes involved in cardiovascular development that are controlled by elements on 22q1.1.

In this study, we describe the chicken ortholog of *DGCR6*. In humans, this gene is located at the most centromeric border of the DiGeorge critical region, and within a 75-kb repeat located more distally (11). *DGCR6*, which shows sequence homology to the *Drosophila* gonadal protein GDL and to the laminin-γ1 chain, has been shown to be deleted in DGS patients, and is highly expressed in heart and striated muscle (33). During murine embryogenesis, *Dgcr6* shows a widespread distribution with highest expression in the pharyngeal arches and central and peripheral nervous system (34). We show in chicken embryos that *DGCR6* is expressed in NCC and their derivatives, like vascular smooth muscle cells and cardiac ganglion cells. Using a retrovirus-based gene delivery system *in vivo*, *DGCR6* expression was disturbed, specifically in premigrating chicken NCC, as has been recently described for *UFD1L* (14). The attenuation of *DGCR6* resulted in cardiovascular anomalies reminiscent of those found in DGS. In addition, expression profiles of *TBX-1*, *UFD1L*, and *HIRA* were analyzed in the pharyngeal arches and in the hearts of treated embryos. *DGCR6* appeared to modify the expression of all three DiGeorge candidate genes in a distinct but transient manner. We conclude that *DGCR6* represses normal *TBX-1* and *UFD1L* expression and stimulates *HIRA*, and may therefore be considered as modifier in the contiguous gene cascade that leads to DGS.

METHODS

Isolation of chicken DGCR6. To isolate chicken *DGCR6*, 10^6 plaque-forming units (pfu) from a chicken heart cDNA library (Stratagene, Heidelberg, Germany) were screened with the human *DGCR6* cDNA (kindly provided by S. Demczuk, Montreal). Four positive clones spanning the complete cDNA were subcloned using the lambda ZAP excision procedure, and were automatically sequenced on both strands. *DGCR6* sequence information is available in the GenBank database (accession number AF048985).

ISH and immunostaining. ^{35}S-based ISH on sections were performed as described previously (35, 36). DIG-based ISH on embryos in whole mount and on sections were essentially performed as described (37), with minor modifications. Briefly, prehybridization treatment included digestion with 10 μg/mL proteinase-K, re-fixation in 4% PFA/0.2% glutaraldehyde, and preincubation in 50% formamide solution containing 5× SSC, 1% SDS, 50 μg/mL tRNA, and 50 μg/mL heparin, at 55°C. Overnight hybridization to DIG-labeled antisense cRNA probes (DIG RNA labeling kit, Roche Molecular Biochemicals, Mannheim, Germany) at 55°C was followed by posthybridization washes and detection with an alkaline phosphatase-conjugated antiserum (1:500, Roche Molecular Biochemicals) and NBT/BCIP staining.

Embryos were fixed with 4% PFA, embedded in paraffin, and sectioned for standard immunohistochemistry with the HNK-1 antibody (Developmental Studies Hybridoma Bank, Iowa City, IA, U.S.A.), tissue culture supernatant diluted 1:20 in PBS with 0.05% Tween-20 and 0.5% BSA. Visualization was performed by incubation with horseradish peroxidase-conjugated rabbit-anti-mouse antiserum (1:200, DAKO, Glostrup, Denmark), followed by staining with 0.04% diaminobenzidine tetrahydrochloride/0.06% H_2O_2 in 0.05 M Tris-maleic acid (pH 7.6).

Retroviral constructs. The pro-retroviral pCXIZ (38) vector was kindly provided by Dr. T. Mikawa (New York, NY, U.S.A.), and was used as backbone for retroviral constructs. Full-length *DGCR6* cDNA (nucl. 117–1247) was cloned in sense and antisense direction between the 5'-long terminal region (LTR) and the IRES (internal ribosomal entry site), which preceded the *LacZ* marker gene and the 3'-LTR of pCXIZ. The partial sense construct for *DGCR6* (nucl. 361–1248) gives rise to an N-terminal truncated product that lacks the putative transmembrane region, inasmuch as translation will start at nucleotide 603. CXL that contains *LacZ* under retroviral LTR control (39) was used as control virus.

All retroviral constructs were stably transfected to the D17.2G helper cell line. *In vivo* infection of premigrating NCC was performed at stage HH9–11, as has been described (5, 7). All animal studies have been approved by the Institutional Review Board. After reincubation embryos were fixed in 4% PFA and stained for the *LacZ* gene product. In conjunction with recent reports (40–42), it appeared that LacZ expression from the IRES-containing retroviral constructs was sparse and tissue specific. To bypass this drawback, the presence of infectious retroviral particles was demonstrated using RT-PCR of *in vitro* incubated R2 rat fibroblasts with i) conditioned medium from nonproducing packaging cells (negative control); ii) conditioned medium from *DGCR6*-antisense retrovirus producing cells (containing *LacZ*); and iii) conditioned medium from CXL producing cells. *In vivo* transduction was demonstrated using cDNA from microdissected hearts (HH24 and HH31), pharyngeal arch mesenchyme (HH 24), and from the proximal parts of the arch arteries (HH31) of infected and control embryos. Total RNA was isolated (RNAzol, Campro-Scientific, Veenendaal, The Netherlands), treated with DNAse-I, and 5 μg was used for random hexamer-primed first-

strand cDNA synthesis. Equal amounts of cDNA were PCR amplified with primers for LacZ (5'- gcgcagcctgaatggcgaatg-3'; 5'-gcaccacagatgaaacgccgag-3'), *DGCR6* (5'-ctgctggagatccagcacc-3'; 5'-catccatcattcgctgctcc-3'), IRES (5'-ccttattccaagcggcttc-3'), and *GAPDH* (5'-gcacgccatcactatcttccag-3'; 5'-ccagacggcaggtcag-gtcacc-3'). All samples were subjected to 35 rounds of PCR (94°C for 30 s, 60°C for 30 s, 72°C for 45 s) with 10 pmol of appropriate primers. To identify the distribution patterns of infected NCC, transduction was performed with a mixture of *DGCR6*-antisense virus and CXL, and with CXL alone, followed by X-gal staining (immersion in PBS containing 10 mM potassium ferricyanide, 10 mM potassium ferrocyanide, 2 mM $MgCl_2$, and 0.1% [wt/vol] X-gal) of the embryos. Migration was distinct and matched the patterns as described for CXL alone.

In vitro demonstration of antisense effect. Constructs were prepared in which full-length *DGCR6* was cloned in sense and antisense orientation at the 3' end of EGFP in the pEGFP-N1 vector (CLONTECH, Palo Alto, CA, U.S.A.). These constructs were used to transfect the packaging cells that produce the sense *DGCR6*-IRES-LacZ carrying retrovirus (see above). Transfection was performed by electroporation of 25,000 cells with 10 μg supercoiled plasmid DNA, by applying one 20-ms pulse of 200V in a 4-mm cuvette (GenePulser Xcell, Bio-Rad, Hercules, CA, U.S.A.). EGFP expression was assessed after 48 h of culture with a fluorescence microscope (Leica Microsystems, Inc., Deerfield, IL, U.S.A.) and the area of expression was determined with Labworks software (UVP Labworks 4.0 (UVP Ltd., Cambridge, U.K.). The area ratios between EGFP-*DGCR6*-antisense and -sense constructs in the packaging cell line were measures for the inhibiting effect of EGFP expression caused by the hybridization of sense and antisense *DGCR6*.

Real-time RT-PCR. Embryos were grouped according to treatment, *i.e.* untreated, CXL, *DGCR6*-antisense, *DGCR6*-partial sense, *DGCR6*-sense (each group $n = 5$), and total RNA was isolated from microdissected hearts and arches of stage HH24 and HH31 embryos (see above). Primer design and SYBR green PCR analysis were performed according to ABI protocols (Applied Biosystems, Foster City, CA, U.S.A.) and run on an ABI PRISM 7700 Sequence Detector (Applied Biosystems). The following primers, 10 pmol of each, were used: *GAPDH* (5'-ggggaaagtcatc-cctgag-3'; 5'-ggcaggtcaggtcaacaac-3'), *TBX-1* (5'-gcactaccacccg-gactc-3'; 5'-cgttatcgtccagcaggtt-3'), *UFD1L* (5'-tcgcaaaggggtagt-gtgt-3'; 5'-gaggcactgtcaccaggag-3'), and *HIRA* (5'-caggc-tgatgatcggagtt-3'; 5'-ccctccacactcgtcaaag-3'). Equal amounts of cDNA (see above) were amplified using 40 PCR cycles of 95°C for 15 s, 60°C for 30 s, and 72°C for 30 s, preceded by a hot start at 95°C for 10 min. Four log dilutions of control cDNA (untreated HH24 embryo) were used to analyze the linearity of amplification ($R^2 > 0.95$) for each set of primers and was included in every analysis as positive control. Melt-down analysis was included to test for aspecific PCR amplicons and was additionally checked by ethidium-bromide–stained agarose gel electrophoresis (no additional products were found; data not shown).

Embryos of the same age group were subjected to analysis of the DiGeorge candidate genes (*TBX-1*, *UFD1L*, and *HIRA*) and *GAPDH* in one and the same real-time RT-PCR run. Crossing of threshold (Ct) values obtained for the experimental genes were normalized against each own *GAPDH* value (43). *t* Test ($p < 0.05$) analysis was applied to test for significance of gene-expression differences between *DGCR6*-retrovirus and CXL treated groups. Values of untreated and CXL-treated groups were not significantly different from each other ($p > 0.95$, not shown). Analyses were repeated three times and no significant interexperimental differences were obtained (not shown).

RESULTS

***Structural analysis of* DGCR6.** We isolated the chicken variant of *DGCR6* (Genbank AF048985; Fig. 1*a*) and show a high degree of conservation between human, mouse, and chicken sequences (Fig. 1*b*). Homology was restricted to residues 280–801 matching 83% with its human (80% on cDNA) and murine homologues (79% on cDNA). Structurally, the predicted protein shows a single transmembrane domain (residues 50–69) predicted by the "DAS"-transmembrane prediction server (http://www.sbe.su.se/~miklos/DAS), a potential tyrosine kinase domain (residues 18–24), and several protein kinase-C phosphorylation sites (residues 76–78, 82–84, and 195–197), suggesting a receptor-like function. N-terminals of the arginine residue at position 18 in chicken, human, and mouse sequences are essentially nonhomologous. Moreover, in the chicken and mouse sequences, the stop loci are conserved, whereas the predicted human peptide is 22 residues longer. Further homology searches revealed minor identity to the *Drosophila* gonadal protein gene *gdl*.

Expression of DGCR6 during chicken embryogenesis. *DGCR6* mRNA is expressed in a variety of cells during the initial stages of chicken development, revealing higher signal in the dorsal part of the neural tube and the mesoderm adjacent to the endoderm (Fig. 2*a*). At HH18, the embryos showed expression in NCC-populated areas, like the pharyngeal arches and the frontonasal mesenchyme (Fig. 2, *b* and *c*). Moreover, the endothelium lining the arch arteries is positive for *DGCR6* (Fig. 2*d*). At HH28, high amounts of *DGCR6* message were found in ectoderm-derived tissues, like the ventral horn of the neural tube, and in neural crest derivatives, such as the spinal ganglia, and the smooth muscle cells of the pharyngeal arch arteries (Fig. 2, *e–h*). At stage HH44, vascular expression was diminished (not shown), and cardiac expression became restricted to the parasympathetic ganglia (Fig. 2, *i–k*), as confirmed by HNK-1 immunostaining (Fig. 2*l*).

Targeting NCC with retroviral DGCR6 constructs. Retroviral constructs carrying antisense and (partial) sense chicken *DGCR6* were prepared and tested *in vitro* for infection properties. Rat fibroblasts were incubated with viral preparations and transduction was demonstrated with RT-PCR (Fig. 3*a*). Transduction *in vivo* was tested similarly by RT-PCR on embryonic tissues. *LacZ* was demonstrated in embryos of which NCC were infected with *DGCR6*-sense and -antisense virus, and with CXL control virus, but not in noninfected embryos (Fig. 3*b*). *In vitro* analysis of inhibition of expression by antisense *DGCR6* showed a 41–53% reduction in EGFP expression upon transfection of cells producing the *DGCR6*-sense retrovirus with the EGFP-*DGCR6*-antisense construct (not shown). Potential disturbance in migration patterning of

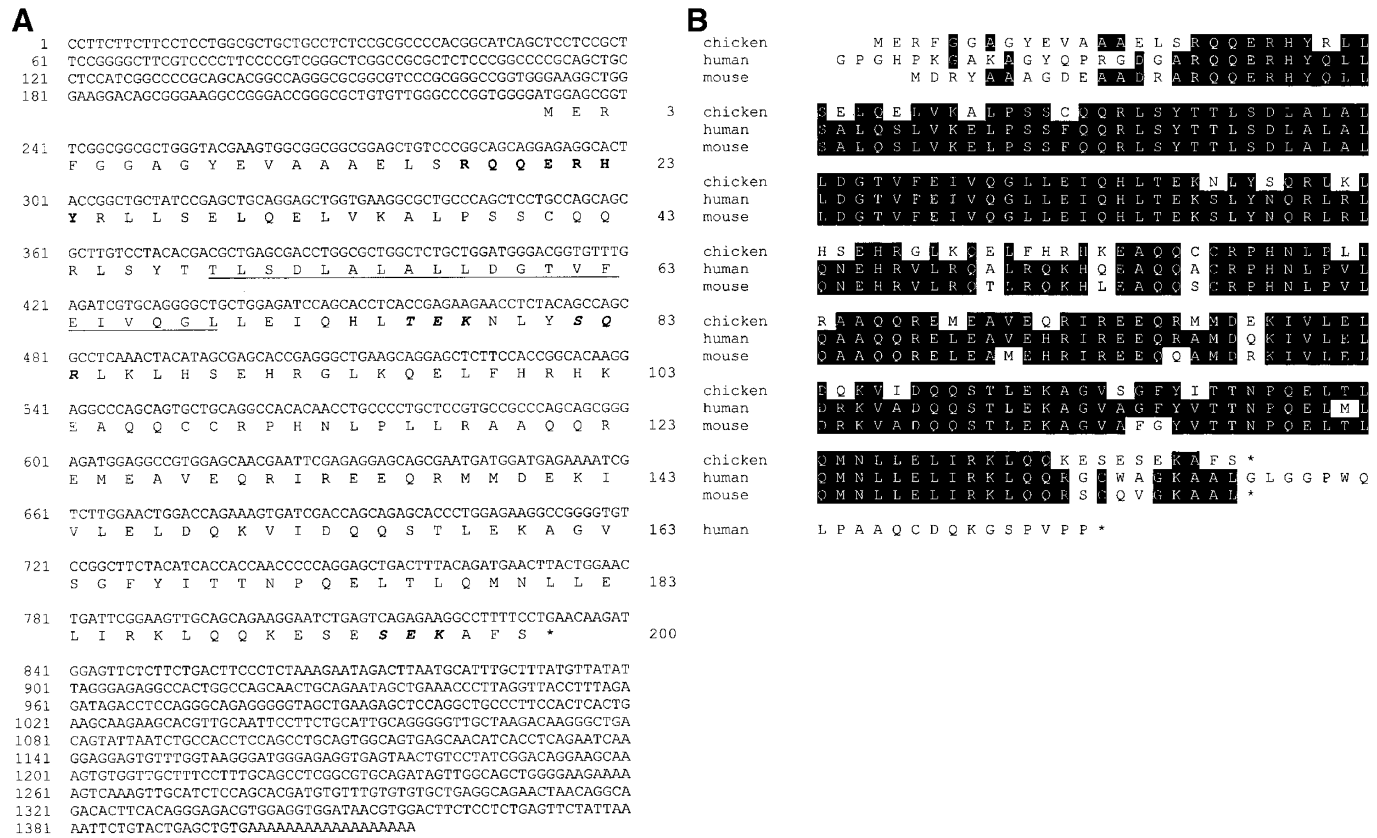

Figure 1. Chicken *DGCR6*. (*a*) cDNA sequence and deduced amino acid sequence of chicken *DGCR6*. A potential tyrosine kinase phosphorylation site is shown in boldface. The underscored sequence represents a putative transmembrane domain. Three potential protein kinase-C domains are italicized in boldface. Chicken *DGCR6* cDNA sequence is available at Genbank (AF048985). (*b*) Alignment of chicken, human (×96484), and murine (AF021031) *DGCR6* protein sequences. Homologous amino acids are boxed. The 5' phosphorylation site and the transmembrane region are conserved.

NCC infected with the *DGCR6*-antisense retrovirus was analyzed by double infection of premigrating NCC with the antisense and CXL viruses. Infected NCC were identified by X-gal staining and staining patterns were compared with those of embryos that were treated with CXL alone (Fig. 3, *c* and *d*). TUNEL analysis on sections of these embryos did not reveal changes in pattern or frequency of apoptosis within infected cell populations (not shown). This shows that the presence of sense or antisense mRNA for *DGCR6* does not affect cell death and migration patterns of NCC.

Cardiovascular morphology upon retroviral infection. Transduction of premigrating NCC with antisense retroviral constructs for *DGCR6*, and with a partial sense construct for *DGCR6*, resulted in a high incidence of severe cardiovascular anomalies (Table 1). These anomalies became apparent during the remodeling stages of the vasculature, *i.e.* from stage HH28 onward, but were never identified earlier. The use of overexpression constructs, *i.e.* full-length sense constructs of which expression was driven by the retroviral promoter elements, as well as *LacZ*-containing control viruses, did not result in the anomalies induced by the attenuation of *DGCR6*. The phenotype designated subarterial ventricular septal defect in the setting of a double outlet of the right ventricle was present in 45% of the embryos treated with *DGCR6*-antisense and in 68% treated with the partial sense construct. It was characterized by an abnormal right-sided position of the aorta (in Fig. 4, compare *a* and *c* with *b* and *d*) and a severely hypoplastic and ventrally displaced ventricular outflow tract septum. The latter resulted in an abnormal communication between left and right ventricles in the outflow segment of the heart up to the semilunar valve level (Fig. 4, *e–h*). No defects above this level, which would be typical for PTA, were found.

Vascular dysmorphic features were present within the group of embryos of which the NCC were transduced with the *DGCR6*-antisense and -partial sense viruses in 16% and 23% of the cases, respectively (Table 1). During normal development, the right ventricle in the avian embryo is bilaterally connected to the dorsal (descending) aorta through the left and right sixth pharyngeal arch arteries. Blood from the left ventricle runs through the right fourth arch artery (ascending aorta) and left and right third arch (brachiocephalic) arteries into the embryo (Fig. 5, *b, d,* and *f*). The left fourth arch artery normally regresses between HH26 and HH31. The most severe end of the spectrum of phenotypes induced by *DGCR6*-antisense or -partial sense transduction included regression of the right fourth arch artery (Fig. 5, *a, c,* and *e*) or anomalous persistence of the left fourth arch artery (not shown). Consistent with DGS and other animal models for this syndrome, especially the fourth, and not the third and sixth arch arteries appeared prone to abnormalities.

DiGeorge gene expression analysis. Real-time RT-PCR analysis was performed to determine gene expression profiles

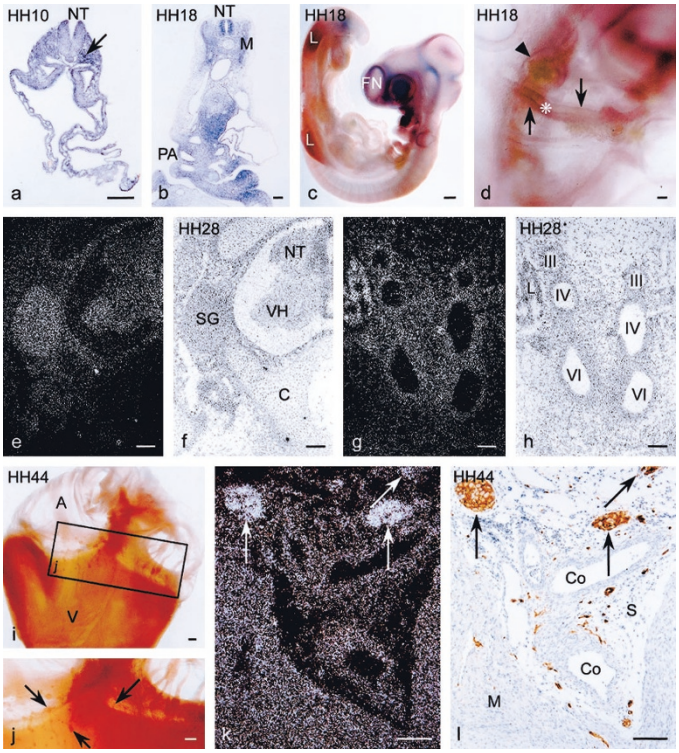

Figure 2. Expression patterns of *DGCR6*. (*a*) ISH for chicken *DGCR6* at stage HH10. Note high expression in the dorsal part of the neural tube (*NT*), and in the lateral mesoderm facing the endoderm (*arrow*). Bar = 10 μm. (*b*) ISH showing high levels of *DGCR6* expression at HH18 in the NT, the myotome (*M*), and in the neural crest derived mesenchyme of the pharyngeal arches (*PA*). Bar = 10 μm. (*c*) At HH18, *DGCR6* expression was found in the eye, the frontonasal mesenchyme (*FN*), and in the limb buds (*L*). Bar = 100 μm. (*d*) *DGCR6* is not only expressed in the PA (*asterisk*), but also in the endothelial lining of the arch arteries (*arrows*), and of the dorsal aorta (*arrowhead*) at HH18. Bar = 10 μm. (*e, f*) Darkfield (*e*) and brightfield (*f*) micrograph of the NT and adjacent tissues at stage HH28. *DGCR6* expression is evident in the spinal ganglia (*SG*), and in the ventral horn (*VH*) of the neural tube ectoderm. *C,* cartilage. Bar = 10 μm. (*g, h*) PA in dark (*g*) and brightfield (*h*) show *DGCR6* expression in the mesenchymal condensations surrounding the third (*III*), fourth (*IV*), and sixth (*VI*) arch arteries. Lung tissue (*L*) is also positive. Bar = 10 μm. (*i, j*) Whole-mount ISH of the HH44 heart, showing *DGCR6* expression in the cardiac ganglia (*arrows*) that are localized in the sulcus mesenchyme between the atria (*A*) and ventricles (*V*). Bar = 100 μm. (*k, l*) ISH for *DGCR6* (*k*) and immunostaining with the HNK-1 antibody that identifies neural crest cells and nervous tissue (*l*) on consecutive sections show co-localization in the cardiac ganglia (*arrows*). *M,* myocardium; *Co,* coronary artery; *s,* sulcus mesenchyme. Bar = 10 μm.

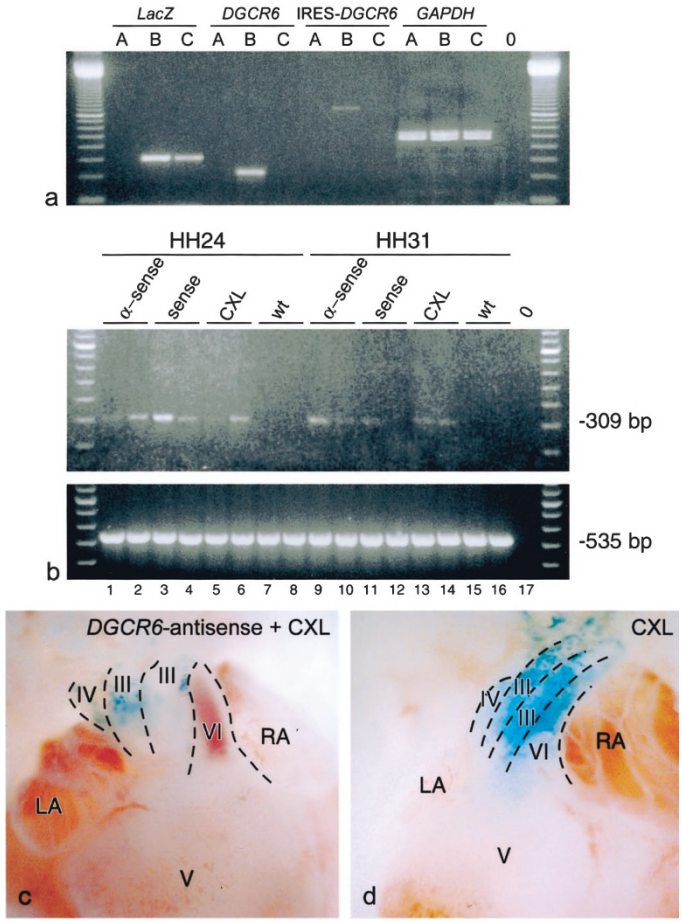

Figure 3. Identification of infectious retroviral particles. (*a*) RT-PCR on RNA from R2 rat fibroblast transduced with conditioned medium from packaging cells producing no virus (*A,* control), *DGCR6*-antisense virus (*B*), and CXL control virus (*C*). Primers for LacZ identified particles in *B* and *C,* whereas primers for *DGCR6* and for IRES-*DGCR6* only amplified from sample *B*. GAPDH primers identified template RNA in all samples. "0" represents sample without template (negative control). (*b*) RT-PCR on RNA samples from embryonic hearts (*odd-numbered lanes*), pharyngeal arch mesenchyme (*lanes 2, 4, 6, 8*), and on pharyngeal arch arteries (*lanes 10, 12, 14, 16*). RNA was isolated from untreated embryos (*wt*), from antisense *DGCR6* (*α-sense*), full-length sense *DGCR6* (*sense*), and CXL treated embryos. 0 = negative control. Primers for LacZ resulted in amplification of a 309-bp product, and for GAPDH in a 535-bp product. (*c, d*) Frontal view on the X-gal stained hearts of stage HH30 embryos of which the NCC were transduced with a mixture of *DGCR6*-antisense and CXL (*c*), and with CXL alone (*d*). X-gal staining shows essentially identical distribution patterns of transduced cells, indicating that the attenuation of *DGCR6* does not result in abnormal NCC migration or cell death.

of three other DiGeorge candidate genes, *TBX-1*, *UFD1L*, and *HIRA* in morphologically affected regions of the heart and arch arteries in *DGCR6*-retrovirus treated embryos. Relative mean expression ratios, *i.e.* expression values normalized to *GAPDH*, are outlined in Figure 6. Compared with CXL control virus treatment, transduction with *DGCR6*-antisense and -partial sense constructs lead to an increase in *TBX-1* and *UFD1L* in the heart and aortic arch mesenchyme at stage HH24 ($p < 0.05$). In contrast, *HIRA* was down-regulated to 63–50% (heart) and 30–0.1% (arches) in these two groups of embryos. The use of *DGCR6*-sense constructs never resulted in significant changes in gene expression, except in the heart at HH24 for *TBX-1* ($p = 0.04$, Fig. 6*a*). However, biologic significance of this small increase, *i.e.* 15% compared with 81% and 93% in *DGCR6*-antisense and -partial sense groups, is unlikely and is underlined by the lack of cardiovascular defects in these embryos. All changes were transient as no significant differences in expression could be measured at HH30, despite perturbed morphology at this stage.

DISCUSSION

Expression and structural aspects of DGCR6. Our results strongly indicate a role for *DGCR6* in cardiovascular development. *DGCR6* was first described (33) as localized to the DiGeorge critical region and as hemizygously deleted in four

Table 1. *Cardiovascular morphology after retroviral infection*

	DGCR6			CXL
	Antisense (n = 31)	Part-sense (n = 22)	Sense (n = 17)	Control (n = 20)
Subarterial VSD/DORV	14 (45%)	15 (68%)	0	0
Absent PAA-IV* (right)	4 (13%)	2 (9%)	0	0
Persistant PAA-IV* (left)	1 (3%)	3 (14%)	0	0

* PAA-IV, fourth pharyngeal arch artery.

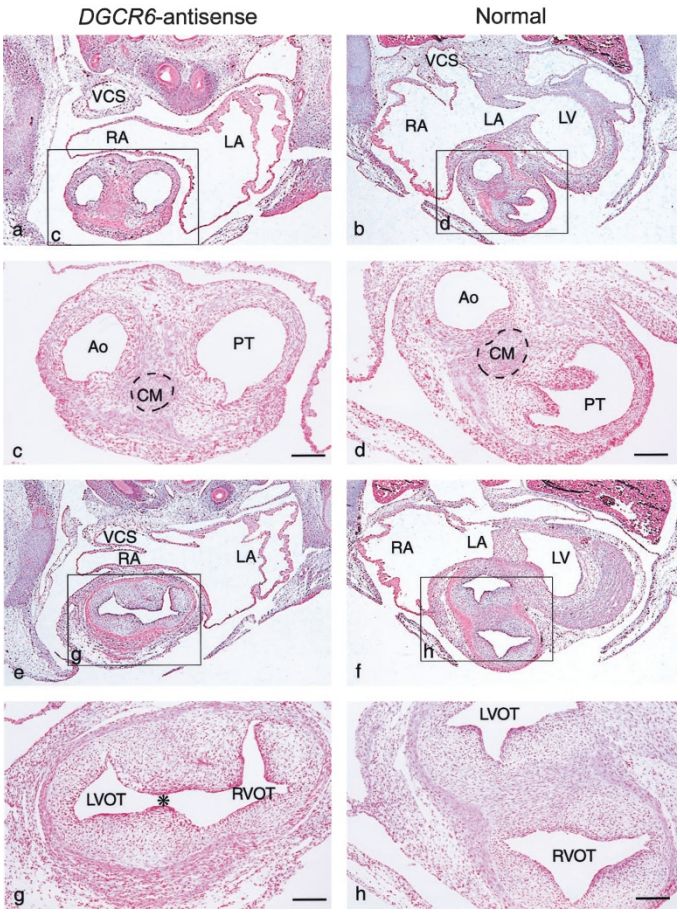

Figure 4. Cardiac anomalies. Sections through the outflow tract at HH31, after transduction with the *DGCR6*-antisense construct (*a, c, e, g*), and control embryos (*b, d, f, h*). Panels *a, b, e, f* are overviews of the heart in which the other panels are marked. (*b, c, d*) Aortic (*Ao*) and pulmonary (*PT*) orifices, just above the level of the semilunar valves, with the NCC-derived condensed mesenchyme (*CM*) normally situated centrally between the orifices (*d*), and malpositioned ventrally after transduction (*c*). (*e, g*) DORV (*asterisk, g*). The left ventricular outflow tract (*LVOT*) connected to the aorta is malpositioned to the right (*g*) compared with the control embryo (*h*), and disconnects to the right ventricular outflow tract (*RVOT*). *RA,* right atrium; *LA,* left atrium; *LV,* left ventricle; *VCS,* superior caval vein. Bar = 10 μm.

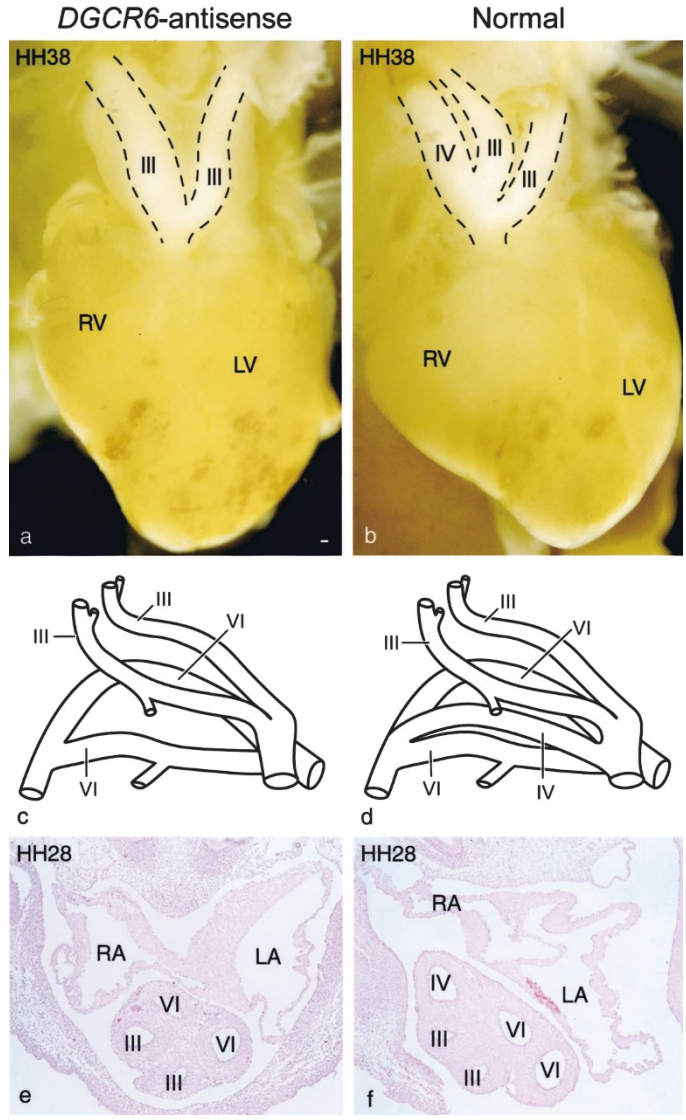

Figure 5. Vascular anomalies. (*a, b*) Frontal view on the heart. Note that the right fourth pharyngeal arch artery (*b*) is missing from the *DGCR6*-antisense transduced embryo (*a*). (*c, d*) Schematic representation of the arch arteries at HH28 showing absence of the right fourth arch artery (*c*). In the normal situation (*d*), blood from the left ventricle runs into a left and right brachiocephalic arteries (*III*) and into a right ascending aorta (*IV*). From the right ventricle the blood runs bilaterally through the sixth arch arteries (arterial ducts) into the dorsal aorta. (*e, f*) Sections through the pharyngeal arch region, showing absence of the right fourth arch artery (*e*), compared with normal (*f*). Bar = 50 μm.

DGS patients. The human gene showed homology to the laminin gamma-1 chain and to the *Drosophila* gonadal protein GDL, of which only homology to the latter was conserved in the chicken sequence of *DGCR6*. The potential single transmembrane domain and phosphorylation sites suggest a receptor-like function for *DGCR6*, but no functional homology to any known receptor family has been found to date. Murine *Dgcr6* was expressed during embryogenesis in the pharyngeal arch mesenchyme and in the central and peripheral nervous system (34). We confirmed these expression data in chicken embryos and, in addition, showed a pattern of expression that was initially broad, but became gradually restricted to neural crest–derived tissues. With respect to cardiovascular development, it is of special interest that the myocardium does not express *DGCR6*, whereas mRNA is abundant during the im-

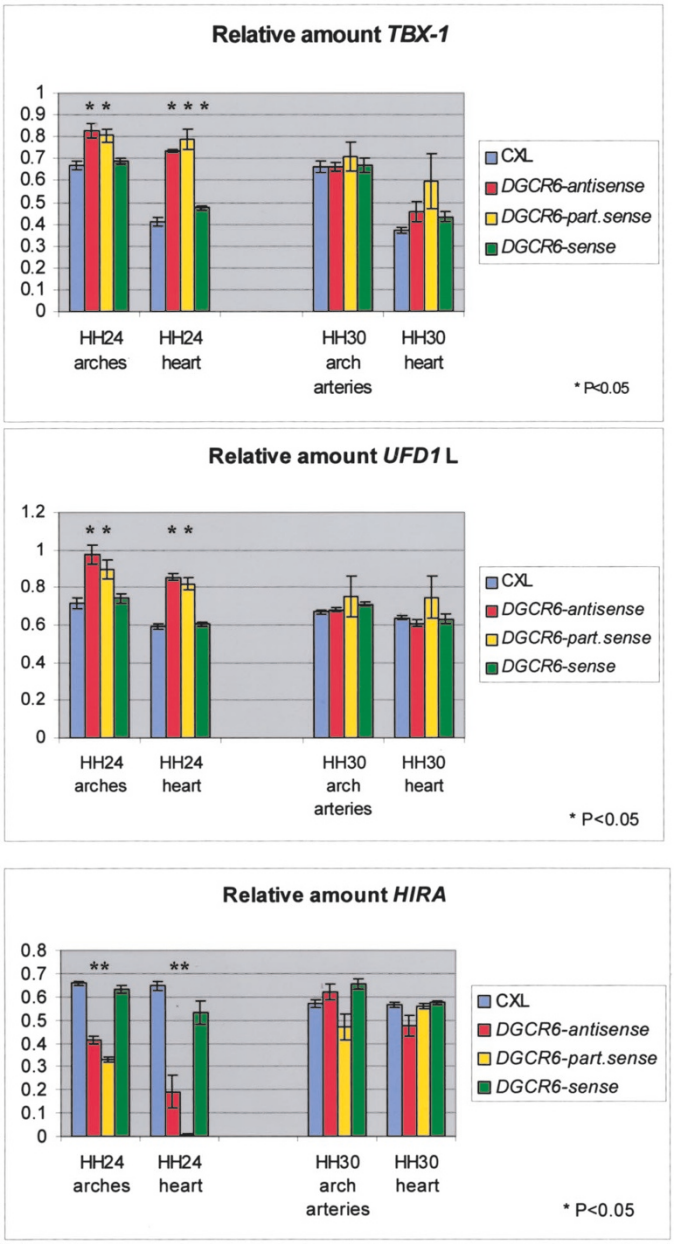

Figure 6. DiGeorge candidate gene expression profiles. Relative expression of *TBX-1*, *UFD1L*, and *HIRA* in hearts and aortic arches at stage HH24 and 30. NCC of stage HH10 embryos were infected with DGCR6-antisense, -partial sense, -sense, or control (*CXL*) retroviruses and embryos ($n = 5$ in each group) were reincubated to stage HH24 or HH30. Hearts and aortic arch mesenchyme (HH24) or arch arteries (HH30) were microdissected and used for real time RT-PCR. From each sample, amplifications were performed for GAPDH and for the gene of interest within one experiment. Ct values were normalized to GAPDH for cDNA input, and means and SEM were calculated. Asterisks (*a–c*) represent the groups that show significant differences (*t* test, $p < 0.05$) of *DGCR6*-retrovirus–treated groups compared with CXL treatment. *TBX-1* and *UFD1L* were transiently up-regulated upon transduction with *DGCR6*-antisense and -partial sense constructs in both arches and hearts. *HIRA*, on the other hand, was down-regulated dramatically in both groups. Transduction with the *DGCR6*-sense construct did not result in changes in expression, except for a slight increase in *TBX-1* in the heart at stage HH24 ($p = 0.037$).

portant stages of pharyngeal arch remodeling. *DGCR6* expression in the arches is not confined to the neural crest–derived mesenchyme, as has been shown, for example, for the endothelin-A receptor (26), or to the mesoderm and epithelia like *Tbx-1* (44). The *DGCR6* expression pattern most closely resembles that of *Ufd1L* (14, 45). It appears that the DiGeorge candidate genes, as described for other genes (46), show distinct and overlapping expression patterns in the pharyngeal arches during crucial stages of vascular remodeling.

Morphology after transduction of NCC with DGCR6. We decided to target *DGCR6* expression *in vivo*, specifically in NCC, by means of a retroviral transduction technique. Recently, we have shown the ability to efficiently target gene expression of the ubiquitin fusion degradation-like protein-1 *UFD1L* (14), and of the transcription factor *ETS* (47) in chicken embryos by retroviral delivery of antisense messages. Transfection data show that expression was reduced to 41–53% upon introduction of an antisense construct for *DGCR6* in an *in vitro* system. This would be in line with the presumed protein levels in a hemizygously deleted DGS patient. CXL-driven *LacZ* markergene expression, as previously shown by our group, has proven its use for NCC transduction and NCC tracing *in vivo* (3–5). Targeting *DGCR6* expression in cardiac NCC using these procedures resulted in abnormal development of the cardiac outflow tract and pharyngeal arch–related vasculature reminiscent to the DiGeorge phenotype.

The cardiac phenotype in our chicken model included subarterial VSD/DORV (45–68%). The neural crest–derived aortopulmonary septum (APS) in these embryos was severely hypoplastic, and did not reach the interventricular septum. Furthermore, because the aorta was malpositioned, the APS was not aligned with the ventricular septum resulting in a persisting left-right communication. This malformation has been described in human patients as a subarterial VSD and appears related to 22q1.1 deletions (8). This in contrast to the "lower" and smaller perimembranous VSD, which are present in deletion patients, but are not indicative for *del22q11.* The development of the fourth pharyngeal arch arteries was severely affected in 16–23% of the embryos, whereas third and sixth arch arteries developed normally. The abnormal persistence of the left and complete absence of the right fourth arch artery suggests that this segment is bilaterally affected. When avian and mammalian vascular development are compared, absence of the right fourth arch artery in chickens equals the type-B interruption of the aortic arch (IAA-B). This phenotype is highly indicative for chromosome 22 deletion syndrome, inasmuch as more than 50% of patients with this phenotype suffer from deletions in 22q11 (8).

It is remarkable that targeting *DGCR6* function in this chicken model results in a similar vascular phenotype as has been described for the $Tbx1^{+/-}$ mouse models (16–18). Whereas the initial specification of the pharyngeal arch arteries appears normal in both chickens and mice (48), the remodeling of the fourth aortic arch artery is seriously hampered, whereas the third and sixth arch arteries develop normally. In addition, in both models the NCC migration patterning appears not to be disturbed (49). This suggests a close relationship between *DGCR6* and *TBX-1* and between NCC and the *TBX-1*-positive surrounding cells during cardiovascular development, possibly through growth factors like Fgf-8 or -10 (24, 50) or VEGF164 (21).

DGCR6 modifies expression of TBX-1, UFD1L, and HIRA. Our data provide the first evidence for a contiguous type of functional interaction between gene products encoded by different genes within the DiGeorge critical region. We showed that interference with *DGCR6* in cardiac NCC influenced the expression levels of *TBX-1*, *UFD1L*, and *HIRA* in the pharyngeal arches and in the heart, even before morphologic anomalies were present. When morphology responds, *i.e.* around HH30, expression levels of these genes have returned to normal. This is in line with the expression profile of *DGCR6* during development. In early development (HH10–HH28), *DGCR6* mRNA was abundantly present in neural crest–populated areas in the embryo like the pharyngeal arches, the frontonasal mesenchyme, and the media of the pharyngeal arch arteries. In these areas, *DGCR6* co-localizes with *UFD1L* (14, 45) and *HIRA* (51), and is present in close proximity to *TBX-1*-positive areas like the endoderm and ectoderm of the pharyngeal pouches and the mesodermal core of the pharyngeal arches (20). Because cardiovascular expression of *DGCR6* becomes restricted to the parasympathetic ganglia on the heart after HH28, the effect of the antisense construct was expected to diminish in the heart and vessels. Apparently, the transient alteration of gene expression during remodeling stages was sufficient for cardiovascular anomalies to develop. The observation that the partial sense construct, based on the originally described *DGCR6* sequence (33), induced the same cardiovascular phenotype and gene expression profile as the antisense construct suggests a dominant negative effect for this gene product. Based on its receptor-like structure, this suggestion appears feasible, as the partial construct codes for an amino-truncated peptide that lacks the potential transmembrane domain and 5' phosphorylation sites and can therefore be considered soluble.

The increase in *TBX-1* and *UFD1L* levels after the attenuation of *DGCR6* indicates a repressor function for DGCR6 during normal development (Fig. 7). On the other hand, the decreases in *HIRA* levels show a positive regulatory mechanism. Considering the expression patterns of *TBX-1* and the fact that *DGCR6* was attenuated in NCC, *DGCR6*-mediated repression should be considered in terms of a cellular interaction mechanism, instead of *cis*- or *trans*-activation of gene expression as has been recently described for the *Tbx-1* promoter (20). Whether that also accounts for *UFD1L* and *HIRA* needs further investigation. A repressor function for *DGCR6* is supported by the mouse models in which parts of chromosome 16, including *Dgcr6*, are deleted (18, 52). These mice do not show cardiovascular anomalies. However, the lack of typical phenotypic DGS characteristics does not rule out involvement of modifier genes, especially of repressors. When *Tbx-1* is homozygously present, the absence of a repressor is not expected to have a major effect. However, when protein levels drop due to hemizygosity, the presence of a repressor could further diminish these levels and worsen the phenotype. In line with this hypothesis the recovery from arterial growth delay, as described by Lindsay and co-workers (48), in the *Df1*/+ mouse model, could be explained by the expression pattern of *DGCR6* and its repressor function on *Tbx-1*, *i.e.* expression of *DGCR6* is high in the smooth muscle cells of the pharyngeal arch arteries around HH28, but diminishes after this stage. This decrease of *DGCR6* in the vessels would relieve the pressure on *TBX-1* expression, allowing a recovery of gene expression and a (partial) restoration of vessel morphology.

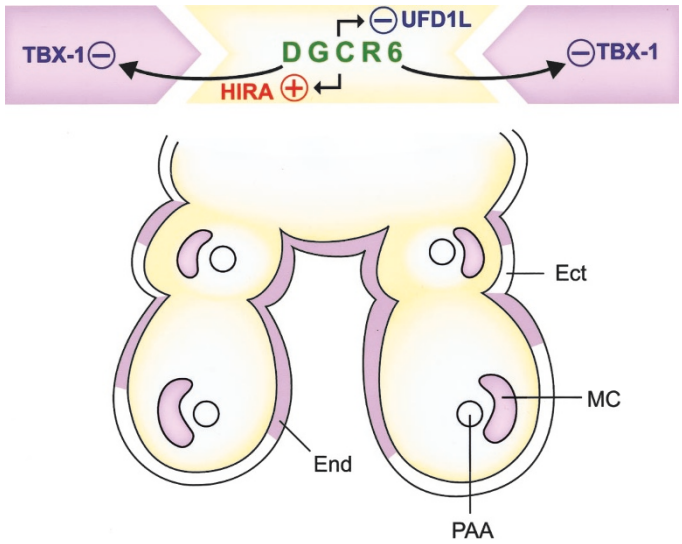

Figure 7. Interaction model in the pharyngeal arch arteries. Hypothetical interaction of *DGCR6* with other DiGeorge candidate genes in the pharyngeal arches during critical phases of cardiovascular remodelling. *DGCR6* is expressed in the neural crest–derived pharyngeal mesenchyme (*yellow*), but not in the ectoderm (*Ect*) or endoderm (*End*). *TBX-1*, on the other hand, shows distinct expression in the latter two structures (*purple*) and in the mesodermal core (*MC*) of the arches. Attenuation of *DGCR6* in NCC results in an up-regulation of *TBX-1* and *UFD1L*, and in down-regulation of *HIRA*. This suggests a repressive effect on *TBX-1* and *UFD1L*, and activation of *HIRA* during normal development. *PAA,* pharyngeal arch artery.

Although a repressor function for *DGCR6* on *TBX-1* would explain several characteristics of described mouse models, it is more difficult to understand why our model, in which *TBX-1* is elevated, evokes a similar phenotype as models in which *Tbx-1* is targeted. However, an increase in *Tbx-1* in the mouse model described by Merscher and co-workers (16) causes defects that are similar to *Tbx-1* haploinsufficiency, as well. Possibly a temporal disbalance in gene expression profiles during critical stages of cardiovascular development is responsible for the described anomalies. On the other hand, the temporal decrease of *UFD1L* and increase of *HIRA* in our model might be instrumental for involvement of additional gene cascades all leading to a similar developmental response. The fact that attenuation of *UFD1L* by the same antisense retrovirus technique in chicken embryos primarily evokes conotruncal anomalies supports this hypothesis (14). Detailed analysis of downstream effectors will be needed to sort out these possibilities.

Acknowledgments. The authors thank Tim Dalebout, Liesbeth van Iperen, and Henri Kerkdijk for expert technical assistance. We also thank Dr. Margot Bartelings for her help in phenotyping, Jan Lens for the artwork, and Dr. Suzanne Demczuk for providing the human *DGCR6* cDNA.

REFERENCES

1. Goldmuntz E, Emanuel BS 1997 Genetic disorders of cardiac morphogenesis. The DiGeorge and velocardiofacial syndromes. Circ Res 80:437–443

2. Erickson CA, Reedy MV 1998 Neural crest development: the interplay between morphogenesis and cell differentiation. Curr Top Dev Biol 40:177–209
3. Poelmann RE, Mikawa T, Gittenberger-de Groot AC 1998 Neural crest cells in outflow tract septation of the embryonic chicken heart: differentiation and apoptosis. Dev Dyn 212:373–384
4. Noden DM, Poelmann RE, Gittenberger-de Groot AC 1995 Cell origins and tissue boundaries during outflow tract development. Trends Cardiovasc Med 5:69–75
5. Bergwerff M, Verberne ME, DeRuiter MC, Poelmann RE, Gittenberger-de Groot AC 1998 Neural crest cell contribution to the developing circulatory system: implications for vascular morphology? Circ Res 82:221–231
6. Kirby ML 1993 Cellular and molecular contributions of the cardiac neural crest to cardiovascular development. Trends Cardiovasc Med 3:18–23
7. Poelmann RE, Gittenberger-de Groot AC 1999 A subpopulation of apoptosis-prone cardiac neural crest cells targets to the venous pole: multiple functions in heart development? Dev Biol 207:271–286
8. Momma K, Matsuoka R, Takao A 1999 Aortic arch anomalies associated with chromosome 22q11 deletion (CATCH 22). Pediatr Cardiol 20:97–102
9. Gittenberger-de Groot AC, Poelmann RE, Bartelings MM 1997 Embryology of congenital heart disease. In: Braunwald E, Freedom R (eds) Congenital Heart Disease. Current Medicine, Philadelphia, pp 3.1–3.10
10. Kurahashi H, Shaikh TH, Hu P, Roe BA, Emanuel BS, Budarf ML 2000 Regions of genomic instability on 22q11 and 11q23 as the etiology for the recurrent constitutional t(11;22). Hum Mol Genet 9:1665–1670
11. Shaikh TH, Kurahashi H, Saitta SC, O'Hare AM, Hu P, Roe BA, Driscoll DA, McDonald-McGinn DM, Zackai EH, Budarf ML, Emanuel BS 2000 Chromosome 22-specific low copy repeats and the 22q11.2 deletion syndrome: genomic organization and deletion endpoint analysis. Hum Mol Genet 9:489–501
12. Llevadot R, Scambler P, Estivill X, Pritchard M 1996 Genomic organization of tuple1/hira: a gene implicated in DiGeorge syndrome. Mamm Genome 7:911–914
13. Yamagishi H, Garg V, Matsuoka R, Thomas T, Srivastava D 1999 A molecular pathway revealing a genetic basis for human cardiac and craniofacial defects. Science 283:1158–1161
14. Yamagishi C, Hierck BP, Gittenberger-de Groot AC, Yamagishi H, Srivastava D 2003 Functional attenuation of Ufd1L, a 22q11.2 deletion syndrome candidate gene, leads to cardiac outflow septation defects in chicken embryos. Pediatr Res 53:546–553
15. Guris DL, Fantes J, Tara D, Druker BJ, Imamoto A 2001 Mice lacking the homologue of the human 22q11.2 gene CRKL phenocopy neurocristopathies of DiGeorge syndrome. Nat Genet 27:293–298
16. Merscher S, Funke B, Epstein JA, Heyer J, Puech A, Lu MM, Xavier RJ, Demay MB, Russell RG, Factor S, Tokooya K, Jore BS, Lopez M, Pandita RK, Lia M, Carrion D, Xu H, Schorle H, Kobler JB, Scambler P, Wynshaw-Boris A, Skoultchi AI, Morrow BE, Kucherlapati R 2001 TBX1 is responsible for cardiovascular defects in velo-cardio-facial/DiGeorge syndrome. Cell 104:619–629
17. Jerome LA, Papaioannou VE 2001 DiGeorge syndrome phenotype in mice mutant for the T-box gene, *Tbx1*. Nat Genet 27:286–291
18. Lindsay EA, Vitelli F, Su H, Morishima M, Huynh T, Pramparo T, Jurecic V, Ogunrinu G, Sutherland HF, Scambler PJ, Bradley A, Baldini A 2001 *Tbx1* haploinsufficieny in the DiGeorge syndrome region causes aortic arch defects in mice. Nature 410:97–101
19. McQuade L, Christodoulou J, Budarf M, Sachdev R, Wilson M, Emanuel B, Colley A 1999 Patient with a 22q11.2 deletion with no overlap of the minimal DiGeorge syndrome critical region (MDGCR). Am J Med Genet 86:27–33
20. Yamagishi H, Maeda J, Hu T, McAnally J, Conway SJ, Kume T, Meyers EN, Yamagishi C, Srivastava D 2003 *Tbx1* is regulated by tissue-specific forkhead proteins through a common Sonic hedgehog-responsive enhancer. Genes Dev 17:269–281
21. Stalmans I, Lambrechts D, De Smet F, Jansen S, Wang J, Maity S, Kneer P, von der Ohe M, Swillen A, Maes C, Gewillig M, Molin DG, Hellings P, Boetel T, Haardt M, Compernolle V, Dewerchin M, Plaisance S, Vlietinck R, Emanuel B, Gittenberger-de Groot AC, Esguerra CV, Scambler P, Morrow B, Driscoll DA, Moons L, Esguerra CV, Carmeliet G, Behn-Krappa A, DeVviendt K, Collen D, Conway SJ, Carmeliet P 2003 VEGF: a modifier of the del22q11 (DiGeorge) syndrome? Nat Med 9:173–182
22. Abu-Issa R, Smyth G, Smoak I, Yamamura K, Meyers EN 2002 Fgf8 is required for pharyngeal arch and cardiovascular development in the mouse. Development 129:4613–4625
23. Frank DU, Fotheringham LK, Brewer JA, Muglia LJ, Tristani-Firouzi M, Capecchi MR, Moon AM 2002 An Fgf8 mouse mutant phenocopies human 22q11 deletion syndrome. Development 129:4591–4603
24. Vitelli F, Taddei I, Morishima M, Meyers EN, Lindsay EA, Baldini A 2002 A genetic link between *Tbx1* and fibroblast growth factor signaling. Development 129:4605–4611
25. Kurihara Y, Kurihara H, Oda H, Maemura K, Nagai R, Ishikawa T, Yazaki Y 1995 Aortic arch malformations and ventricular septal defect in mice deficient in endothelin-1. J Clin Invest 96:293–300
26. Clouthier DE, Hosoda K, Richardson JA, Williams SC, Yanagisawa H, Kuwaki T, Kumada M, Hammer RE, Yanagisawa M 1998 Cranial and cardiac neural crest defects in endothelin-A receptor-deficient mice. Development 125:813–824
27. Yanagisawa H, Yanagisawa M, Kapur RP, Richardson JA, Williams SC, Clouthier DE, de Wit D, Emoto N, Hammer RE 1998 Dual genetic pathways of endothelin-mediated intercellular signaling revealed by targeted disruption of endothelin converting enzyme-1 gene. Development 125:825–836
28. Bartram U, Molin DG, Wisse LJ, Mohamad A, Sanford LP, Doetschman T, Speer CP, Poelmann RE, Gittenberger-de Groot AC 2001 Double-outlet right ventricle and overriding tricuspid valve reflect disturbances of looping, myocardialization, endocardial cushion differentiation, and apoptosis in TGFβ2-knockout mice. Circulation 103:2745–2752
29. Iida K, Koseki H, Kakinuma H, Kato N, Mizutani-Koseki Y, Ohuchi H, Yoshioka H, Noji S, Kawamura K, Kataoka Y, Ueno F, Taniguchi M, Yoshida N, Sugiyama T, Miura N 1997 Essential roles of the winged helix transcription factor MFH-1 in aortic arch patterning and skeletogenesis. Development 124:4627–4638
30. Winnier GE, Kume T, Deng K, Rogers R, Bundy J, Raines C, Walter MA, Hogan BL, Conway SJ 1999 Roles for the winged helix transcription factors MF1 and MFH1 in cardiovascular development revealed by nonallelic noncomplementation of null alleles. Dev Biol 213:418–431
31. Franz T 1989 Persistent truncus arteriosus in the Splotch mutant mouse. Anat Embryol (Berl) 180:457–464
32. Feiner L, Webber AL, Brown CB, Lu MM, Jia L, Feinstein P, Mombaerts P, Epstein JA, Raper JA 2001 Targeted disruption of semaphorin 3C leads to persistent truncus arteriosus and aortic arch interruption. Development 128:3061–3070
33. Demczuk S, Thomas G, Aurias A 1996 Isolation of a novel gene from the DiGeorge Syndrome critical region with homology to Drosophila *gdl* and to human *LAMC1* genes. Hum Mol Genet 5:633–638
34. Lindsay EA, Baldini A 1997 A mouse gene (Dgcr6) related to the Drosophila gonadal gene is expressed in early embryogenesis and is the homolog of a human gene deleted in DiGeorge syndrome. Cytogenet Cell Genet 79:243–247
35. Hierck BP, Poelmann RE, van Iperen L, Brouwer A, Gittenberger-de Groot AC 1996 Differential expression of α6 and other subunits of laminin binding integrins during development of the murine heart. Dev Dyn 206:100–111
36. Hierck BP, Gittenberger-de Groot AC, van Iperen L, Brouwer A, Poelmann RE 1996 Expression of the beta-4 integrin subunit in the mouse heart during embryonic development: retinoic acid advances beta-4 expression. Dev Dyn 207:89–103
37. Wilkinson DG 1995 RNA detection using non-radioactive *in situ* hybridization. Curr Opin Biotechnol 6:20–23
38. Mima T, Ueno H, Fischman DA, Williams LT, Mikawa T 1995 Fibroblast growth factor receptor is required for *in vivo* cardiac myocyte proliferation at early embryonic stages of heart development. Proc Natl Acad Sci U S A 92:467–471
39. Mikawa T, Fischman DA, Dougherty JP, Brown AM 1991 *In vivo* analysis of a new lacZ retrovirus vector suitable for cell lineage marking in avian and other species. Exp Cell Res 195:516–523
40. Cohen-Tannoudji M, Vandormael-Pournin S, Drezen J, Mercier P, Babinet C, Morello D 2000 lacZ sequences prevent regulated expression of housekeeping genes. Mech Dev 90:29–39
41. Lau S, Jardine K, McBurney MW 1999 DNA methylation pattern of a tandemly repeated LacZ transgene indicates that most copies are silent. Dev Dyn 215:126–138
42. Vagner S, Galy B, Pyronnet S 2001 Irresistible IRES: attracting the translation machinery to internal ribosome entry sites. EMBO Rep 2:893–898
43. Pfaffl MW 2001 A new mathematical model for relative quantification in real-time RT- PCR. Nucleic Acids Res 29:e45
44. Chapman DL, Garvey N, Hancock S, Alexiou M, Agulnik SI, Gibson-Brown JJ, Cebra-Thomas J, Bollag RJ, Silver LM, Papaioannou VE 1996 Expression of the T-box family genes, *Tbx1-Tbx5*, during early mouse development. Dev Dyn 206:379–390
45. Pizzuti A, Novelli G, Ratti A, Amati F, Mari A, Calabrese G, Nicolis S, Silani V, Marino B, Scarlato G, Ottolenghi S, Dallapiccola B 1997 Ufd1l, a developmentally expressed ubiquitination gene, is deleted in CATCH 22 syndrome. Hum Mol Genet 6:259–265
46. Clouthier DE, Williams SC, Yanagisawa H, Wieduwilt M, Richardson JA, Yanagisawa M 2000 Signaling pathways crucial for craniofacial development revealed by endothelin-A receptor-deficient mice. Dev Biol 217:10–24
47. Lie-Venema H, Gittenberger-de Groot AC, van Empel LJ, Boot MJ, Kerkdijk H, de Kant E, DeRuiter MC 2003 Ets-1 and Ets-2 transcription factors are essential for normal coronary and myocardial development in chicken embryos. Circ Res 92:749–756
48. Lindsay EA, Baldini A 2001 Recovery from arterial growth delay reduces penetrance of cardiovascular defects in mice deleted for the DiGeorge syndrome region. Hum Mol Genet 10:997–1002
49. Vitelli F, Morishima M, Taddei I, Lindsay EA, Baldini A 2002 Tbx1 mutation causes multiple cardiovascular defects and disrupts neural crest and cranial nerve migratory pathways. Hum Mol Genet 11:915–922
50. Kochilas L, Merscher-Gomez S, Lu MM, Potluri V, Liao J, Kucherlapati R, Morrow B, Epstein JA 2002 The role of neural crest during cardiac development in a mouse model of DiGeorge syndrome. Dev Biol 251:157–166
51. Roberts C, Daw SC, Halford S, Scambler PJ 1997 Cloning and developmental expression analysis of chick Hira (Chira), a candidate gene for DiGeorge syndrome. Hum Mol Genet 6:237–245
52. Puech A, Saint-Jore B, Merscher S, Russell RG, Cherif D, Sirotkin H, Xu H, Factor S, Kucherlapati R, Skoultchi AI 2000 Normal cardiovascular development in mice deficient for 16 genes in 550 kb of the velocardiofacial/DiGeorge syndrome region. Proc Natl Acad Sci U S A 97:10090–10095